

Ellipsoidal collapse and an improved model for the number and spatial distribution of dark matter haloes

Ravi K. Sheth¹, H. J. Mo¹ & Giuseppe Tormen²

¹ *Max-Planck Institut für Astrophysik, 85740 Garching, Germany*

² *Dipartimento di Astronomia, 35122 Padova, Italy*

Submitted 1 July 1999

ABSTRACT

The Press–Schechter, excursion set approach allows one to make predictions about the shape and evolution of the mass function of bound objects. The approach combines the assumption that objects collapse spherically with the assumption that the initial density fluctuations were Gaussian and small. While the predicted mass function is reasonably accurate at the high mass end, it has more low mass objects than are seen in simulations of hierarchical clustering. We show that the discrepancy between theory and simulation can be reduced substantially if bound structures are assumed to form from an ellipsoidal, rather than a spherical collapse. In the original, standard, spherical model, a region collapses if the initial density within it exceeds a threshold value, δ_{sc} . This value is independent of the initial size of the region, and since the mass of the collapsed object is related to its initial size, this means that δ_{sc} is independent of final mass. In the ellipsoidal model, the collapse of a region depends on the surrounding shear field, as well as on its initial overdensity. In Gaussian random fields, the distribution of these quantities depends on the size of the region considered. Since the mass of a region is related to its initial size, there is a relation between the density threshold value required for collapse, and the mass of the final object. We provide a fitting function to this $\delta_{ec}(m)$ relation which simplifies the inclusion of ellipsoidal dynamics in the excursion set approach. We discuss the relation between the excursion set predictions and the halo distribution in high resolution N-body simulations, and use our new formulation of the approach to show that our simple parametrization of the ellipsoidal collapse model represents a significant improvement on the spherical model on an object-by-object basis. Finally, we show that the associated statistical predictions, the mass function and the large scale halo-to-mass bias relation, are also more accurate than the standard predictions.

Key words: galaxies: clustering – cosmology: theory – dark matter.

1 INTRODUCTION

Current models of galaxy formation assume that structure grows hierarchically from small, initially Gaussian density fluctuations. Collapsed, virialized dark matter haloes condense out of the initial fluctuation field, and it is within these haloes that gas cools and stars form (White & Rees 1977; White & Frenk 1991; Kauffmann et al. 1999). In such models, understanding the properties of these dark haloes is important. There is some hope that dark haloes will be relatively simple to understand, because, to a good approximation, gravity alone determines their properties. The formation and other properties of dark haloes can be studied using both N-body simulations and analytical models. The most developed analytic model, at present, has come

to be called the Press–Schechter approach. It allows one to compute good approximations to the mass function (Press & Schechter 1974; Bond et al. 1991), the merging history (Lacey & Cole 1993, 1994; Sheth 1996; Sheth & Lemson 1999b) and the spatial clustering (Mo & White 1996; Mo, Jing & White 1996, 1997; Catelan et al. 1998; Sheth 1998; Sheth & Lemson 1999a) of dark haloes.

Let $n(m, z)$ denote the number density of bound objects that have mass m at time z . Press & Schechter (1974) argued that collapsed haloes at a late time could be identified with overdense regions in the initial density field. Bond et al. (1991) described how the assumption that objects form by spherical collapse could be combined with fact that the initial fluctuation distribution was Gaussian, to predict $n(m, z)$. To do so, they made two assumptions: (i) a region

collapses at time z if the initial overdensity within it exceeds a critical value, $\delta_{\text{sc}}(z)$. This critical value depends on z , but is independent of the initial size of the region. The dependence of δ_{sc} on z is given by the spherical collapse model. (ii) the Gaussian nature of the fluctuation field means that a good approximation to $n(m, z)$ is given by considering the barrier crossing statistics of many independent, uncorrelated random walks, where the barrier shape $B(m, z)$ is given by the fact that, in the spherical model, δ_{sc} is independent of m .

While the mass function predicted by this ‘standard’ model is reasonably accurate, numerical simulations show that it may fail for small haloes (Lacey & Cole 1994; Sheth & Tormen 1999). This discrepancy is not surprising, because many assumptions must be made to arrive at reasonably simple analytic predictions. In particular, the spherical collapse approximation to the dynamics may not be accurate, because we know that perturbations in Gaussian density fields are inherently triaxial (Doroshkevich 1970; Bardeen et al. 1986).

In this paper, we modify the standard formalism by incorporating the effects of non-spherical collapse. In Section 2 we argue that the main effect of including the dynamics of ellipsoidal rather than spherical collapse is to introduce a simple dependence of the critical density required for collapse on the halo mass. There is some discussion in the literature as to why the excursion set approach works. Section 3 continues this, and shows that our simple change to the ‘standard’ model reduces the scatter between the predicted and actual masses of haloes on an object-by-object basis. Section 4 shows that this simple change also substantially improves the agreement between predicted statistical quantities (the halo mass function and halo-to-mass bias relations) and the corresponding simulation results. A final section summarizes our findings, and discusses how they are related to the work of Monaco (1995), Bond & Myers (1996), Audit, Teyssier & Alimi (1997), and Lee & Shandarin (1998).

2 THE EXCURSION SET APPROACH

The first part of this section summarizes the ‘standard’ model in which the spherical collapse model is combined with the assumption that the initial fluctuations were Gaussian and small. The second part shows how the ‘standard’ model can be modified to incorporate the effects of ellipsoidal, rather than spherical, collapse.

2.1 Spherical collapse: the constant barrier

Let $\sigma(r)$ denote the rms fluctuation on the scale r . In hierarchical models of clustering from Gaussian initial fluctuations, σ decreases as r increases in a way that is specified by the power spectrum. If the initial fluctuations were small, then the mass m within a region of size r is just $m \propto r^3$. Bond et al. (1991) argued that the mass function of collapsed objects at redshift z , $n(m, z)$, satisfies

$$\nu f(\nu) \equiv m^2 \frac{n(m, z)}{\bar{\rho}} \frac{d \log m}{d \log \nu}, \quad (1)$$

where $\bar{\rho}$ is the background density, $\nu = \delta_{\text{sc}}(z)/\sigma(m)$ is the ratio of the critical overdensity required for collapse in the

spherical model to the rms density fluctuation on the scale r of the initial size of the object m , and the function of the left hand side is given by computing the distribution of first crossings, $f(\nu) d\nu$, of a barrier $B(\nu)$, by independent, uncorrelated Brownian motion random walks. Thus, in their model, for Gaussian initial fluctuations, $n(m, z)$ is determined by the shape of the barrier, $B(\nu)$, and by the relation between the variable ν and the mass m (i.e., by the initial power spectrum).

Bond et al. used the spherical collapse model to determine the barrier height B as a function of ν as follows. In the spherical collapse model, the critical overdensity $\delta_{\text{sc}}(z)$ required for collapse at z is independent of the mass m of the collapsed region, so it is independent of $\sigma(m)$. Therefore, Bond et al. argued that since $\nu \equiv (\delta_{\text{sc}}/\sigma)$, then $B(\nu)$ must be the same constant for all ν . Using the spherical collapse model to set $\delta_{\text{sc}}(z)$ means, e.g., that $B = \delta_{\text{sc}}(z) = 1.68647(1+z)$ in an Einstein-de Sitter universe. Since the barrier height associated with the spherical collapse model does not depend on $\nu = (\sigma_*/\sigma)$, and since the random walks are assumed to be independent and uncorrelated, the first crossing distribution can be derived analytically. This allowed Bond et al. (1991) to provide a simple formula for the shape of the mass function that is associated with the dynamics of spherical collapse:

$$\nu f(\nu) = 2 \left(\frac{\nu^2}{2\pi} \right)^{1/2} \exp \left(-\frac{\nu^2}{2} \right). \quad (2)$$

Notice that in this approach, the effects of the background cosmology and power spectrum shape can be neatly separated. The cosmological model determines how δ_{sc} depends on z , whereas the shape of the power spectrum fixes how the variance depends on scale r , so it fixes how σ depends on mass $m \propto r^3$. Furthermore, for scale free spectra, if the mass function is well determined at one output time, then the others can be computed by simple rescalings.

In this excursion set approach, the shape of the mass function is determined by $B(\sigma)$ and by $\sigma(m)$. Since $\sigma(m)$ depends on the shape of the initial power spectrum but not on the underlying dynamics, to incorporate the effects of ellipsoidal collapse into the excursion set model, we only need to determine the barrier shape associated with the new, non-spherical dynamics. Below, we describe a simple way to do this.

2.2 Ellipsoidal collapse: the moving barrier

The gravitational collapse of homogeneous ellipsoids has been studied by Icke (1973), White & Silk (1979), Peebles (1980), and Lemson (1993). We will use the model in the form described by Bond & Myers (1996). That is, the evolution of the perturbation is assumed to be better described by the initial shear field than the initial density field, initial conditions and external tides are chosen to recover the Zel'dovich approximation in the linear regime, and virialization is defined as the time when the third axis collapses. This last choice means that there is some freedom associated with how each axis is assumed to evolve after turnaround, and is the primary free parameter in the model we will describe below. Following Bond & Myers (1996), we have chosen the following prescription. Whereas, in principle, an axis may collapse

to zero radius, collapse along each axis is frozen once it has shrunk by some critical factor. This freeze-out radius is chosen so that the density contrast at virialization is the same (179 times the critical density) as in the spherical collapse model. The results which follow are not very sensitive to the exact value of this freeze out radius.

For a given cosmological background model (we will study the Einstein-de Sitter case in detail below), the evolution of an ellipsoidal perturbation is determined by three parameters: these are the three eigenvalues of the deformation tensor, or, equivalently, the initial ellipticity e , prolateness p , and density contrast δ (our e and p are what Bond & Myers 1996 called e_v and p_v , and are defined so that $|p| \leq e$. See Appendix A for details). Figure 1 shows the expansion factor at collapse as a function of e and p , for a region that had an initial overdensity $\delta = 0.04215$, in an Einstein-de Sitter universe. At a given e , the largest circles show the relation at $p = 0$, medium sized circles show $|p| \leq e/2$, and the smallest circles show $|p| \geq e/2$. On average, virialization occurs later as e increases, and, at a given e , it occurs later as p decreases. For an Einstein-de Sitter model the linear theory growth factor is proportional to the expansion factor, so this plot can be used to construct $\delta_{\text{ec}}(e, p)$. For the range of e and p that are relevant for the results to follow, a reasonable approximation to this relation is given by solving

$$\frac{\delta_{\text{ec}}(e, p)}{\delta_{\text{sc}}} = 1 + \beta \left[5(e^2 \pm p^2) \frac{\delta_{\text{ec}}^2(e, p)}{\delta_{\text{sc}}^2} \right]^\gamma \quad (3)$$

for $\delta_{\text{ec}}(e, p)$, where $\beta = 0.47$, $\gamma = 0.615$, δ_{sc} is the critical spherical collapse value, and the plus(minus) sign is used if p is negative(positive). [If $\gamma = 0.5$ then this relation can be solved analytically to provide some feel for how δ_{ec} depends on e and p . For example, when $\gamma = 0.5$ and $p = 0$, then $\delta_{\text{ec}} \approx \delta_{\text{sc}}/(1 - e)$.] The solid curve in Fig. 1 shows the value given by equation (3) when $\gamma = 0.615$ for $p = 0$, and the two dashed curves show $|p| = e/2$.

We want to consider the collapse of ellipsoids from an initially Gaussian fluctuation field. Appendix A shows that on any scale R_f parameterized by $\sigma(R_f)$, there is a range of probable values of e , p and δ . This means that there is a range of collapse times associated with regions of size R_f . In principal, we could obtain an estimate for an average $\delta_{\text{ec}}(\sigma)$ by averaging $\delta_{\text{ec}}(e, p)$ over $p(e, p, \delta/\sigma)$ suitably. In essence, Monaco (1995), Audit, Teyssier & Alimi (1997) and Lee & Shandarin (1998) give different prescriptions for doing this. We will use the simpler procedure described below.

On average in a Gaussian field, $p = 0$. The solid curve in Fig. 1 shows the expansion factor at virialization in this case. It is straightforward to use this curve to compute the associated $\delta_{\text{ec}}(e, z)$. Having done so, if we can relate e to the mass m , then we will be in a position to describe the barrier shape associated with ellipsoidal, rather than spherical collapse. This can be done as follows. Regions initially having a given value of δ/σ most probably have an ellipticity $e_{\text{mp}} = (\sigma/\delta)/\sqrt{5}$ (see Appendix). To collapse and form a bound object at z , the initial overdensity of such a region must have been $\delta_{\text{ec}}(e_{\text{mp}}, z)$. If we require that δ on the right hand side of this relation for e_{mp} be equal to this critical value $\delta_{\text{ec}}(e_{\text{mp}}, z)$, then this sets $\sigma^2(R_f)$. Since R_f^3 is proportional to mass, this provides a relation between e and mass, and so between δ_{ec} and mass:

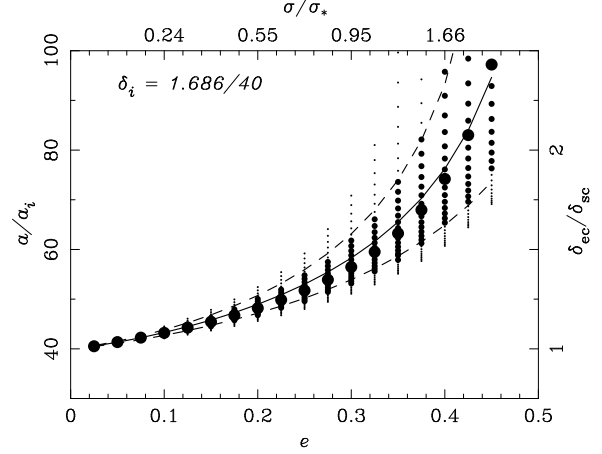


Figure 1. The evolution of an ellipsoidal perturbation in an Einstein-de Sitter universe. Symbols show the expansion factor when the longest axis collapses and virializes, as a function of initial e and p , in steps of 0.025, if the initial overdensity was δ_i . The solid curve shows our simple formula for the $p = 0$ result, and the dashed curves show $|p| = e/2$. The time required to collapse increases monotonically as p decreases. The axis on the right shows the associated critical overdensity required for collapse, and the axis on the top shows the result of using our simple formula to translate from e to $\sigma(m)$ when $p = 0$.

$$\delta_{\text{ec}}(\sigma, z) = \delta_{\text{sc}}(z) \left(1 + \beta \left[\frac{\sigma^2}{\sigma_*^2(z)} \right]^\gamma \right), \quad (4)$$

where we set $\sigma_*(z) \equiv \delta_{\text{sc}}(z)$. The axis labels on the top and right of the plot show this ($p = 0$) relation.

Notice that the power spectrum enters only in the relation between σ and m , whereas the effects of cosmology enter only in the relation between δ_{sc} and z . For example, this expression is approximately the same for Λ CDM, OCDM, and Λ CDM models if all variances $\sigma^2(m)$ are computed using the model dependent power spectrum, and the value of $\delta_{\text{sc}}(z)$ is computed using the spherical collapse model after including its dependence on background cosmology: the differences between these models arise primarily from converting the scaling variable ν to the physical variables z and m .

A number of features of equation (4) are worth noticing. Massive objects have $\sigma/\sigma_* \ll 1$. For such objects equation (4) suggests that $\delta_{\text{ec}}(\sigma, z) \approx \delta_{\text{sc}}(z)$, so the critical overdensity required for collapse at z is approximately independent of mass: massive objects are well described by the spherical collapse model. Other approaches yield the same result (e.g., Bernardeau 1994). Second, the critical overdensity increases with $\sigma(m)$, so it is larger for less massive objects. This is because smaller objects are more influenced by external tides; they must have a greater internal density if they are to hold themselves together as they collapse.

Equation (4) is extremely useful because it allows one to include the effects of ellipsoidal collapse into the Bond et al. (1991) excursion set model in a straightforward manner. Namely, all we need to do is to use equation (4) when setting $B(\sigma, z) = \delta_{\text{ec}}(\sigma, z)$. Then the distribution of first crossings of this barrier by independent random walks can be used to give an estimate of the mass function associated with ellipsoidal collapse. For example, it is straightforward

to simulate an ensemble of independent unconstrained random walks, and to record the distribution of first crossings of the ellipsoidal collapse ‘moving’ barrier. To a very good approximation, this first crossing distribution is

$$\nu f(\nu) = 2A \left(1 + \frac{1}{\nu^{2q}}\right) \left(\frac{\nu^2}{2\pi}\right)^{1/2} \exp\left(-\frac{\nu^2}{2}\right), \quad (5)$$

where ν was defined earlier, $q = 0.3$ and $A \approx 0.3222$. This first crossing distribution differs from that predicted by the ‘standard’ constant barrier model (equation 2) for which $q = 0$ and $A = 1/2$.

The great virtue of interpreting equation (4) as the ‘moving’ barrier shape is that, once the barrier shape is known, all the predictions of the excursion set program can be computed relatively easily. This means that we can use the logic of Lacey & Cole (1993) to compute the conditional mass functions associated with ellipsoidal rather than spherical collapse. As in the original model, this is given by considering the successive crossing of boundaries associated with different redshifts. Once this conditional mass function is known, the forest of merger history trees can be constructed using the algorithm described by Sheth & Lemson (1999b), from which the nonlinear stochastic biasing associated with this mass function can be derived using the logic of Mo & White (1996) and Sheth & Lemson (1999a).

3 EXCURSION SET PREDICTIONS AND N-BODY SIMULATIONS

The mass function in equation (2) was first derived by Press & Schechter (1974). They used the Gaussian statistics of regions which are denser than $\delta_{\text{sc}}(z)$ on a given scale $\sigma(m)$ to compute the mass function of haloes at redshift z . However, their derivation did not properly address what happens to regions which are denser than $\delta_{\text{sc}}(z)$ on more than one scale. The excursion set approach of Bond et al. (1991) shows how to do this. It is based on the following hypothesis: at z , the mass of a collapsed object is the same as the mass within the largest region in the initial conditions that could have collapsed at z .

Unfortunately, this hypothesis makes no reference to the centre of the collapsed object, either in the initial conditions or at the final time, whereas the Bond et al. calculation does. This has led to some discussion in the literature as to exactly how one should compare the excursion set approach predictions with the haloes which form in numerical simulations of hierarchical clustering. These discussions have led to the perception that, on an object-by-object basis, the excursion set predictions are extremely unreliable (Bond et al. 1991; White 1996), so that it is difficult to explain why, in a statistical sense, the excursion set predictions work as well as they do (Monaco 1999). This section provides a discussion of how the predictions of this approach are related to the results of numerical simulations. It then shows that the excursion set approach does, in fact, make accurate predictions, even on an object-by-object basis. This comparison shows that, on an object-by-object basis, our parametrization of ellipsoidal dynamics represents a significant improvement on the standard spherical model.

3.1 Selecting haloes in the initial conditions

Suppose that our statement of the excursion set hypothesis is correct: the largest region in the initial conditions that can collapse, will. Then it should be possible to combine the spherical collapse model with the statistics of the initial fluctuation field to obtain an estimate of the mass function of haloes at z . The natural way to do this is as follows. Generate the initial Gaussian random fluctuation field. Compute the average density within concentric spherical regions centred on each position of the field. These are the excursion set trajectories associated with each position. At each position, find the largest spherical region within which the initial average density fluctuation exceeds $\delta_{\text{sc}}(z)$. Call the mass within this region the predicted mass. Thus, for each position in the initial field, there is an associated $m_{\text{pred}}(z)$. Go to the position with the largest $m_{\text{pred}}(z)$, call this position r_1 and set $m_1 = m_{\text{pred}}$. Associated with m_1 is a spherical volume $v_1 = m_1/\bar{\rho}$ centred on r_1 . Disregard the predicted masses (i.e. ignore the excursion set trajectories) for all the other positions within this v_1 . If the simulation box has volume V , consider the remaining volume $V - v_1$. Set m_2 equal to the largest value of $m_{\text{pred}}(z)$ in the remaining volume $V - v_1$, and record this position r_2 . Disregard the predicted mass for all other positions within the associated v_2 . Continue until the remaining volume in the simulation box is as small as desired. The resulting list of m_i s represents the halo mass function predicted by the excursion set approach. The list of positions r_i represents the Lagrangian space positions of the haloes. This is essentially the algorithm described at the end of Section 3.3 in Bond & Myers (1996). (They also describe what to do in the event that, for example, some of the mass associated with v_2 was within v_1 .) Inclusion of ellipsoidal, rather than spherical dynamics, into this excursion set algorithm is trivial: simply replace δ_{sc} with $\delta_{\text{ec}}(m)$.

Although this algorithm follows naturally from the excursion set hypothesis, in practice, it is rather inefficient. For this reason, making a preliminary selection of candidate positions for the excursion set r_i s may be more efficient. For example, whereas the algorithm described above selects peaks in the initial m_{pred} distribution, the positions of these peaks may correspond to peaks in the density field itself. Since these may be easier to identify, it may be more efficient to use them instead. Essentially, this is the motivation behind the peak-patch approach of Bond & Myers (1996).

3.2 Predicted and actual halo masses

The algorithm described above shows that the only values of m_{pred} that are relevant are those that are in the list of m_i s. That is, only a few stalks in the bundle of excursion set trajectories are actually associated with collapsed objects. It is easy to understand why. Imagine running a numerical simulation. Choose a random particle in the simulation, and record the mass m of the halo in which this particle is at some specified redshift z . Since the particle was chosen at random, it is almost certainly not the centre-of-mass particle of the halo in which it is at z . Is there a simple reason why the halo collapsed around the centre-of-mass particle, and not around the one chosen at random? The excursion set answer to this question is ‘yes’: collapse occurs around positions which are initially local maxima of the excursion

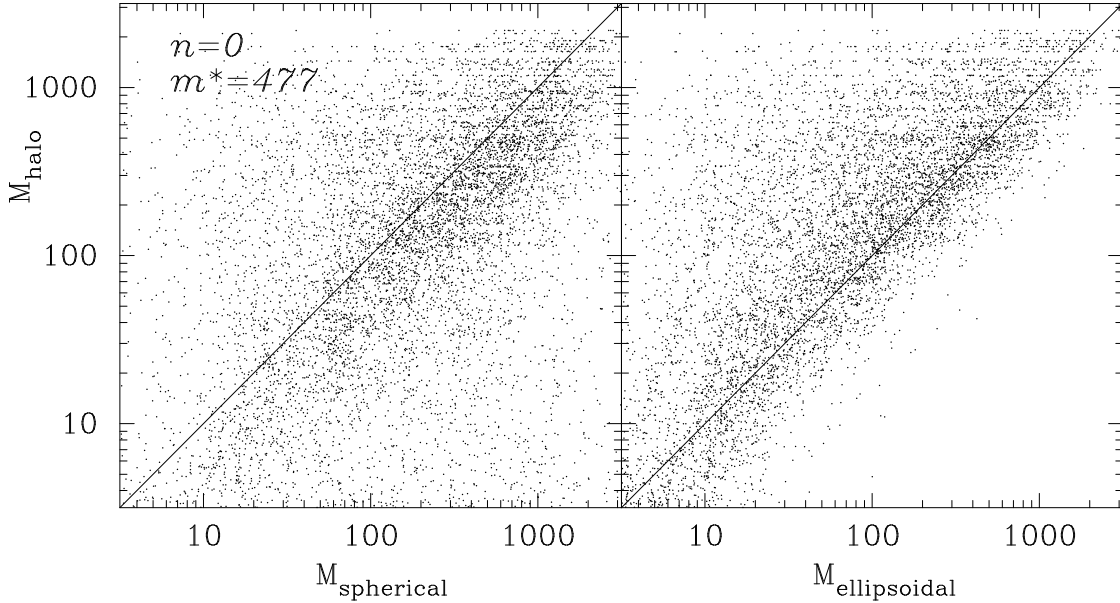


Figure 2. The mass of the halo in which a randomly chosen particle is, M_{halo} , is plotted versus the mass predicted by the spherical (left panel) and ellipsoidal collapse (right panel) models. A randomly chosen 10^4 of the 10^6 particles in a simulation of an Einstein-de Sitter universe with white noise initial conditions were used to make the plot.

set predicted mass. When collapse occurs, the approach assumes that shells do not cross, so initially concentric shells remain concentric. This means that the centre-of-mass particle at the final time is also the centre-of-mass particle initially (particles retain the binding energy ranking they had in the initial conditions), and that the predicted mass for this centre-of-mass particle is higher than for the one chosen at random. This has the important consequence that only the centre-of-mass particle prediction is a good estimate for the mass of the halo at z ; all other particles provide underestimates of the final mass.

We will use Figures 2–4 to demonstrate this in two steps. First, we will use Figure 2 to argue that ellipsoidal dynamics represents a significant improvement over the spherical model. Then, we will use Figures 3 and 4 to show that our moving barrier excursion set approach associated with ellipsoidal dynamics allows one to make accurate predictions on an object-by-object basis. These figures were constructed using numerical simulations which were kindly made available by Simon White, and are described in White (1996). They follow the clustering of 10^6 particles from white noise initial conditions (of course, the results to follow are similar for other initial power spectra). We have chosen to show results for that output time ($a/a_i = 36$) in the simulations in which the number of haloes containing more than ten particles each was $\sim 10^4$. This number was chosen for ease of comparison with Fig. 8 of White (1996).

To show that the evolution of an object is well described by spherical or ellipsoidal dynamics, we should compare the evolution of the object’s three axes with that of the model. For the spherical model, this has been done by Lemson (1995). We will perform a cruder test here. In the spherical collapse model, an object forms at z if the initial overdensity within it exceeds $\delta_{\text{sc}}(z)$. Since, in the model, shells do not cross, so initially concentric regions remain concentric, we can compare $M_{\text{predicted}}$, the mass contained within

the largest spherical region centred on a randomly chosen particle in the initial conditions within which the density exceeds $\delta_{\text{sc}}(z)$, with M_{halo} , the mass of the object in which that particle actually is at z . The comparison with ellipsoidal dynamics is similar, except that one uses $\delta_{\text{ec}}(M_{\text{halo}})$, instead of the spherical collapse value, to compute the predicted mass. Thus, rather than testing the detailed evolution of the object, this simply tests whether or not the time it takes before virialization occurs depends on the initial overdensity in the way the model describes.

Figure 2 shows this comparison for 10^4 particles chosen randomly from the simulation. (We use the same set of particles in both panels. For cosmetic reasons, the predicted mass has been shifted randomly within each mass bin as described by White.) The panel on the left shows the scatter plot associated with spherical dynamics (it should be compared with White’s plot, which was constructed from a simulation with $n = -1$ initial conditions), and the panel on the right shows the result of using our parametrization of ellipsoidal dynamics instead. Namely, the y position associated with a particle is given by M_{halo} , the mass of the halo in which the particle is, and the x position is obtained as we described above.

The difference between the two panels is striking: the points in the panel on the right populate the upper left half only. This difference is easily understood: whereas, δ_{sc} is independent of M_{halo} , $\delta_{\text{ec}}(m)$ increases as m decreases. Therefore, relative to the spherical model, the largest filter size containing the critical ellipsoidal collapse overdensity decreases as M_{halo} decreases, so that $M_{\text{ellipsoidal}} \leq M_{\text{spherical}}$ always. Thus, in effect, including ellipsoidal dynamics moves all the points in the spherical model scatter plot to the left, and, on average, this shift depends on M_{halo} .

White (1996) argued that such a scatter plot could be used to test the excursion set approach. He argued that if the Bond et al. (1991) formulation of the excursion set ap-

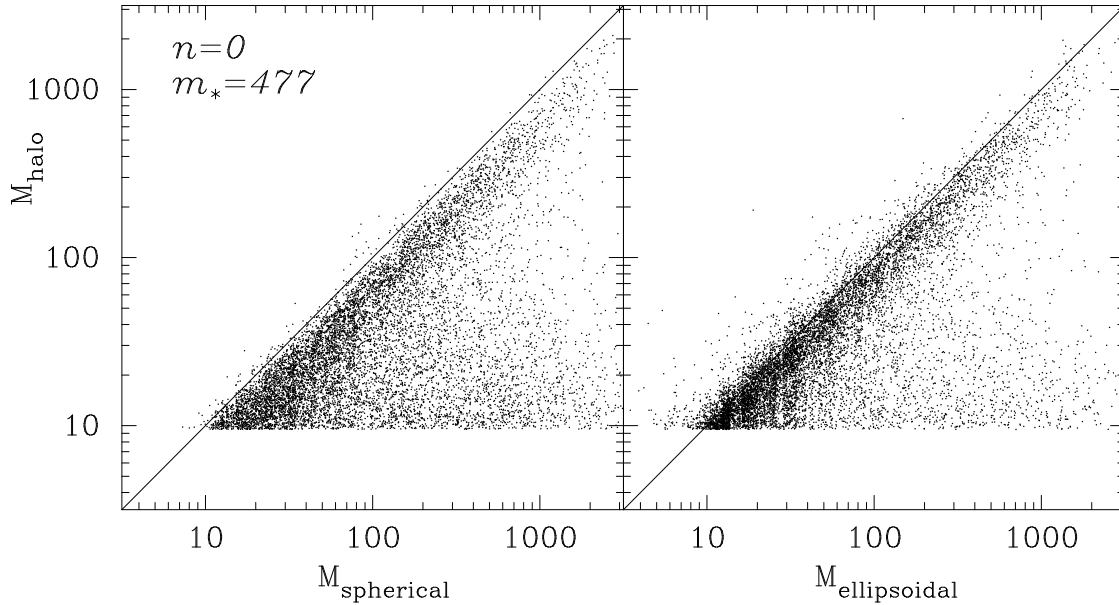


Figure 3. The mass of a halo in a simulation of an Einstein-de Sitter universe with white noise initial conditions versus that predicted by the excursion set approach. The panel on the left shows the prediction associated with the ‘standard’ spherical collapse approximation to the dynamics; the panel on the right shows the prediction associated with our moving barrier parametrization of the ellipsoidal collapse model.

proach is correct, then there should be no scatter in such a plot. Figure 2 shows that, although the correlation between M_{halo} and $M_{\text{predicted}}$ is tighter in the ellipsoidal than in the spherical model, the scatter in both panels is still considerable. That this scatter is, in fact, quite large led White to argue that the accuracy of the excursion set predictions was surprising.

However, as we discussed above, much of this scatter is a consequence of choosing random particles to construct the scatter plot. We argued that because random particles will almost always provide an underestimate of the true mass, such a plot should be populated only in the upper left half. This is clearly not the case for spherical dynamics (the panel on the left). Whereas the panel on the right looks more like we expect, it is not really a fair test of the ellipsoidal collapse, moving barrier, excursion set model, because it was constructed using a fixed $\delta_{\text{ec}}(M_{\text{halo}})$, rather than one which depends on scale, to compute $M_{\text{predicted}}$. Using the scale dependent $\delta_{\text{ec}}(m)$ relation, rather than the fixed value $\delta_{\text{ec}}(M_{\text{halo}})$, to construct the plot will have the effect of moving some of the points to the right. Nevertheless, this panel suggests that inclusion of ellipsoidal dynamics represents a significant improvement over the spherical model.

To make this point more clearly, Fig. 3 shows the scatter plot one obtains by using only those particles which are centres of haloes to make the comparison between theory and simulations. (Only haloes containing more than 10 particles were used to make this plot, since discreteness effects in the initial conditions become important on the small scales initially occupied by less massive haloes). As before, the panel on the left shows the result of using spherical dynamics to compute the predicted mass, and the one on the right shows the one associated with ellipsoidal dynamics—but now, the predicted mass is computed using the ellipsoidal collapse moving barrier, rather than one fixed at the value associ-

ated with M_{halo} . The most striking difference between this plot and the previous one is that now the upper left half in both panels is empty. As we discussed above, this provides strong support for our excursion set assumption that collapse occurs around local maxima of the m_{pred} distribution.

In addition to showing the correlation, on an object-by-object basis, between predicted and simulated masses more clearly, using only the centre of mass particles when constructing the scatter plot allows us to test the relative merits of the spherical and ellipsoidal model approximations to the exact dynamics. In both panels, some of the discrepancy between prediction and simulation arise if some of the mass predicted to be in a halo was already assigned to a halo of larger mass, because $M_{\text{pred}} > M_{\text{halo}}$ produces points which populate the bottom right half of the plot. However, in the ellipsoidal model, some of the discrepancy almost certainly arises from the fact that we use a very simple prescription for relating the mass to e and p . Presumably, the scatter in the panel on the right can be reduced by explicitly computing $\delta_{\text{ec}}(e, p)$, and using this to compute $M_{\text{ellipsoidal}}$, rather than by using the representative value e_{mp} that we adopted when deriving equation (4).

Fig. 4 shows the result of accounting for the effects of this scatter in the following crude way. The initial region containing the mass of M_{halo} could have had different values of e and p than the ones we assumed. Since δ_{ec} is a function of e and p , changing these values results in a different predicted $M_{\text{ellipsoidal}}$. The lines through each point in the figure illustrate the range of predicted masses associated with each object if the ellipsoidal collapse barrier in equation (4) had $|p| = \pm 0.33e$. On any given scale, integrating $g(e_{\text{mp}}, p|\delta)$ over this range in p (recall $e_{\text{mp}} = (\sigma/\delta)/\sqrt{5}$), shows that p falls in this range approximately 50% of the time (and in the range $|p|/e = 0.5$, 70% of the time). For clarity, of the $\sim 10^4$ objects, only a randomly chosen five

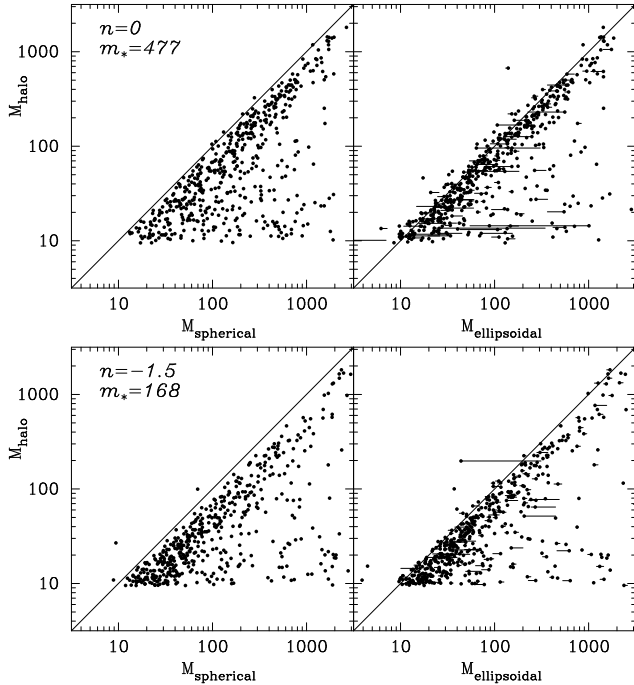


Figure 4. The effect of changing p at a given e on the predicted mass of a halo: as p becomes more negative(positive), $\delta_{ec}(e, p)$ increases(decreases), so the predicted mass decreases(increases). The filled circles show the $p = 0$ prediction used to produce the previous figure, and the bars show the range $|p| = 0.33e$. The two panels on the top show the result for white noise initial conditions, and the bottom panels were constructed from simulations in which the slope of the initial power spectrum was $n = -1.5$.

hundred are shown. The plot shows the correlation more clearly than the previous figure. It also shows that, at least for some of the objects, the difference between the predicted and actual masses may be attributed to the scatter in initial values of e and p . We have not pursued this in further detail.

We feel that, taken together, the three figures above make two points. Firstly, because the upper left half of the scatter plot for centre-of-mass particles really is empty, our excursion set hypothesis that collapse occurs around local maxima of the m_{pred} distribution must be quite accurate. Secondly, because the centre-of-mass points follow the $M_{\text{halo}} = M_{\text{predicted}}$ relation reasonably well, and because the scatter around this mean relation is smaller for the ellipsoidal than for spherical dynamics predictions, our parametrization of ellipsoidal dynamics in the excursion set approach represents a significant improvement on the spherical model, on an object-by-object basis.

We also think it important to point out that our model requires that collapse have occurred along all three axes. Had we chosen collapse along only the first axis to signify virialization, $\delta_{ec}(m)$ would decrease with m . In this case, $M_{\text{ellipsoidal}} \geq M_{\text{spherical}}$, and including ellipsoidal dynamics would increase the scatter in Fig. 2. Moreover, all points in the left panel of Fig. 3 would be shifted to the right, with points having small M_{halo} being shifted further. Thus, if there were any correlation between the predicted and simulated masses in the resulting scatter plot, it would not be along the $M_{\text{halo}} = M_{\text{predicted}}$ line. Therefore, Figs. 2–4 provide strong empirical justification for our identification of

virialization with the time at which all three axes of the initial ellipsoid collapse.

Finally, because the centre-of-mass particles really do show the expected correlation, if one is interested in studying the statistical properties of collapsed objects, then it should be a good approximation to study only these centre-of-mass particles. For example, suppose one is interested in using the fact that the initial distribution was a Gaussian random field to predict the fraction of mass which is contained in objects which have collapsed along all three axes. Since only 8% of all positions in an initial Gaussian field are predicted to collapse along all three axes (e.g. Lee & Shandarin 1998) one might conclude that only 8% of the mass can be contained in such objects. However, just as the only relevant excursion set predictions are those associated with centre-of-mass trajectories (in our model the excursion set trajectories and associated predictions centred on other positions, while almost surely wrong, are irrelevant), so also is this value of 8%, because it is based on the statistics of random positions, a very misleading number. The relevant question is not what fraction of all positions can collapse along all three axes, but what fraction of centre-of-mass particles (or, equivalently, peaks in the initial m_{pred} distribution) can collapse along all three axes. This fraction is almost certainly closer to unity than to 8%. Moreover, since each such particle may be at the centre of a collapsed halo that has a mass considerably greater than that of a single particle, the actual fraction of mass that is in objects that have collapsed along all three axes can be considerable. Since these centre-of-mass particles are almost certainly not randomly placed in the initial field, this fraction is more difficult to estimate, though it is certainly considerably greater than 8%.

This is also why computing other statistical quantities, such as the mass function of collapsed objects, is more complicated. Substituting the first crossing distribution associated with the ellipsoidal collapse moving barrier (equation 5) in equation (1) to compute the mass function is equivalent to assuming that the statistics of randomly chosen particles are the same as those of centre-of-mass particles. This is not an unreasonable first approximation. (We plan to present a more detailed derivation of the relation between the first crossing distribution associated with independent random excursion set trajectories and the mass function associated with centre-of-mass trajectories in a separate paper. The more detailed derivation shows that this simple approximation is also reasonably accurate.) This approximation gives the original Press-Schechter, Bond et al. (1991) formula for the mass function associated with spherical collapse, and equation (5) for the mass function associated with our parametrization of ellipsoidal collapse.

4 STATISTICAL PREDICTIONS

This section provides two examples of the increase in accuracy of the predicted statistical quantities that results from the inclusion of ellipsoidal dynamics in the excursion set approach.

4.1 The mass function

Fig. 2 of Sheth & Tormen (1999) shows that, in the GIF (Kauffmann et al. 1999) simulations of clustering in SCDM, OCDM and Λ CDM models, the unconditional mass function is well approximated by

$$\nu f(\nu) = 2A \left(1 + \frac{1}{\nu'^{2q}}\right) \left(\frac{\nu'^2}{2\pi}\right)^{1/2} \exp\left(-\frac{\nu'^2}{2}\right), \quad (6)$$

where $\nu' = \sqrt{a}\nu$, $a = 0.707$, $q = 0.3$ and $A \approx 0.322$ is determined by requiring that the integral of $f(\nu)$ over all ν give unity (this last just says that all the mass is assumed to be in bound objects of some mass, however small). Essentially, the factor of $a = 0.707$ is determined by the number of massive haloes in the simulations, and the parameter q is determined by the shape of the mass function at the low mass end. The GIF mass function differs from that predicted by the ‘standard’ model (equation 2) for which $a = 1$, $q = 0$, and $A = 1/2$. The simulations have more massive haloes and fewer intermediate and small mass haloes than predicted by equation (2). Comparison with equation (5) shows that the two expressions are identical, except for the factor of a .

To show this more clearly, we can derive numerically (following Sheth 1998) the shape of the barrier $B(\sigma, z)$ which gives rise to the GIF mass function of equation (6), if the relation between the first crossing distribution $f(\sigma)d\sigma$ of independent unconstrained Brownian walks and the halo mass function is given by equation (1). Since the random walk problem can also be phrased in terms of the scaled variable ν , and since the GIF mass functions can also be expressed in this variable, we only need to compute the barrier shape once; simple rescaling of the variables gives the barrier shape at all later times. To a very good approximation, the barrier associated with the GIF simulations has the form

$$B_{\text{GIF}}(\sigma, z) = \sqrt{a}\delta_{\text{sc}}(z) \left(1 + b \left[\frac{\sigma^2}{a\sigma_*^2(z)}\right]^c\right), \quad (7)$$

where $\delta_{\text{sc}}(z) = \sigma_*(z)$, $\sigma(m)$ and a are the same parameters that appear in the mass function, so $\delta_{\text{sc}}(z)$ is given by the spherical collapse model and depends on the cosmological model, $\sigma(m)$ depends on the shape of the initial fluctuation spectrum, $\sigma/\sigma_*(z) \equiv \sigma(m)/\delta_{\text{sc}}(z) \equiv 1/\nu$, $b = 0.5$, and $c = 0.6$. Notice that this barrier shape (equation 7) which is required to yield the GIF mass function (equation 6) has the same functional form as the barrier shape associated with the ellipsoidal collapse model (equation 4). Except for the factor of a , the two barriers are virtually identical.

To some extent, the value of a is determined by how the haloes were identified in the simulations. There is some freedom in how one this is done. Typically, one uses a friends-of-friends or spherical overdensity algorithm to identify bound groups. Both algorithms have a free parameter which is usually set by using the spherical collapse model. In the spherical overdensity case, the overdensity is usually set to ~ 200 times the background density. In the friends-of-friends case, it is customary to set the link-length to 0.2 times the mean interparticle separation. Clearly, the shape of the mass function will depend on how groups are identified. In the friends-of-friends case, for example, decreasing the link-length will result in fewer massive objects. Since we are considering the mass function associated with collapsed ellipsoids, it is not

obvious any more that the free parameters in these group finders should be set using the spherical collapse values.

Consider what happens as we change the link-length in the friends-of-friends case. If, on average, the density profile of the objects identified using a given link-length is a power law, then decreasing the link-length means that all haloes will become less massive by some multiplicative factor. If this power law is approximately independent of halo mass, then this factor will also be approximately independent of halo mass. This means that, for some range of scales, there is a degeneracy between the friends-of-friends link-length and the parameter M_* . Since the mass function in the simulations is a function of σ/σ_* , this will translate into a degeneracy between the link length and M_* , so the degeneracy between link length and σ_* may depend on power spectrum. For this reason, we will treat the parameter a in equation (6) above as being related to the link-length. The value $a = 0.707$ is that associated with a link-length which is 0.2 times the mean interparticle separation, the value suggested by the spherical collapse model, when the power spectrum is from the CDM family. Presumably, if we were to decrease this link-length sufficiently, we would find $a \approx 1$. Since the link-length associated with $a = 0.707$ is more or less standard, we have not changed it and recomputed the simulation mass function. Rather, we have simply chosen to argue that the fact that the GIF barrier (equation 7) is simply a scaled version of the moving barrier of equation (4) argues strongly in support of the accuracy of the ellipsoidal collapse model.

4.2 Biasing on large scales

The large scale halo-to-mass bias relation in simulations is also different from that predicted by the ‘standard’ spherical collapse model (Jing 1998, 1999; Sheth & Lemson 1999a; Porciani, Catelan & Lacey 1999; Sheth & Tormen 1999). Fig. 5 shows this large scale bias relation as a function of halo mass for haloes which form from initially scale free Gaussian random density fluctuation fields: i.e., the initial power spectrum was $P(k) \propto k^n$. The dotted line shows Jing’s (1998) fit to this bias relation, measured in numerical simulations of hierarchical clustering. The dashed line shows the bias relation computed by Mo & White (1996) using the ‘standard’ spherical collapse, constant barrier model. While it is reasonably accurate at the high mass end, the less massive haloes in the simulations appear to cluster more strongly than this model predicts. Sheth & Tormen (1999) argued that some of this discrepancy arises from the fact that the mass function in the simulations differs from the Press–Schechter function. They combined the simulation mass function with the peak background split approximation to estimate the large scale bias. If the rescaled mass function in Jing’s scale free simulations is the same as that in the GIF simulations, then their peak background split formula fares better than the standard model, though it does not produce the upturn at low masses that Jing finds. Moreover, Sheth & Tormen gave no dynamical justification for why the mass function differs from the standard one.

To compute the large scale bias relation associated with our ellipsoidal collapse, moving barrier model we must relate the bias relation to the random walk model. This was been done by Mo & White (1996), who argued that the bias

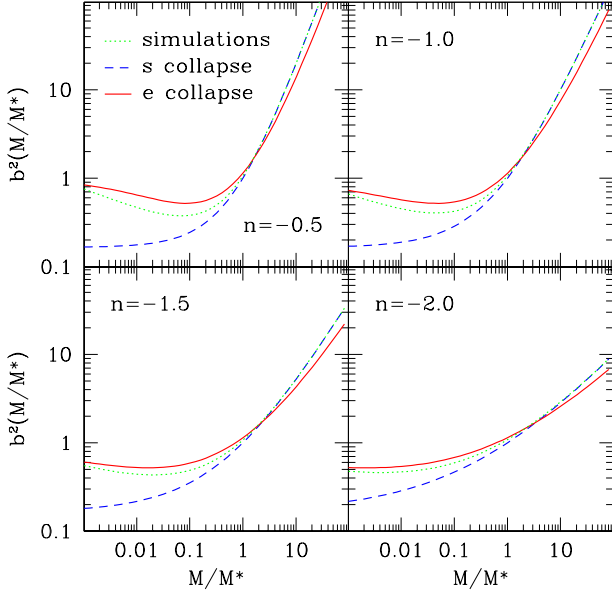


Figure 5. The large scale bias factor $b(m)$ as a function of halo mass. Dotted curves show a fit to this relation measured in numerical simulations by Jing (1998), though his Figure 3 shows that the bias factor for massive haloes in his simulations is slightly smaller than the one given by his fitting function. Dashed curves show the spherical collapse prediction of Mo & White (1996), and solid curves show the ellipsoidal collapse prediction of this paper. At the high mass end, our solid curves and the simulation results differ from Jing’s fitting function (dotted) in the same qualitative sense.

relation was related to the crossing of two barriers (also see Sheth & Tormen 1999). Essentially, the large scale bias relation is associated with random walks which travel far from the origin before intersecting the barrier. To insure that this happens, one must consider random walks which intersect the barrier when the barrier height is very high. We have simulated random walks, and recorded the first crossings of the barrier given in equation (7) in the high-barrier limit. We have then used the relation given by Mo & White to compute the associated prediction for the large scale bias relation. To a very good approximation, this relation is

$$b_{\text{Eul}}(\nu) = 1 + b_{\text{Lag}}(\nu),$$

where $\nu \equiv \delta_{\text{sc}}(z)/\sigma(m, z)$, and

$$b_{\text{Lag}}(\nu) = \frac{1}{\sqrt{a}\delta_{\text{sc}}(z)} \left[\sqrt{a}(a\nu^2) + \sqrt{a}b(a\nu^2)^{1-c} - \frac{(a\nu^2)^c}{(a\nu^2)^c + b(1-c)(1-c/2)} \right], \quad (8)$$

where a , b and c are the same parameters that describe the barrier shape (equation 7). The solid curve shows the predicted large scale Eulerian bias relation (with $a = 0.707$, $b = 0.5$ and $c = 0.6$); it produces an upturn at the low mass end that is similar to the one seen in Jing’s simulations. (In practice, the mass functions in the initial scale free simulations differ slightly from the GIF mass function. So, strictly speaking, the bias relation should be computed using the values of a , b and c associated with the actual mass function

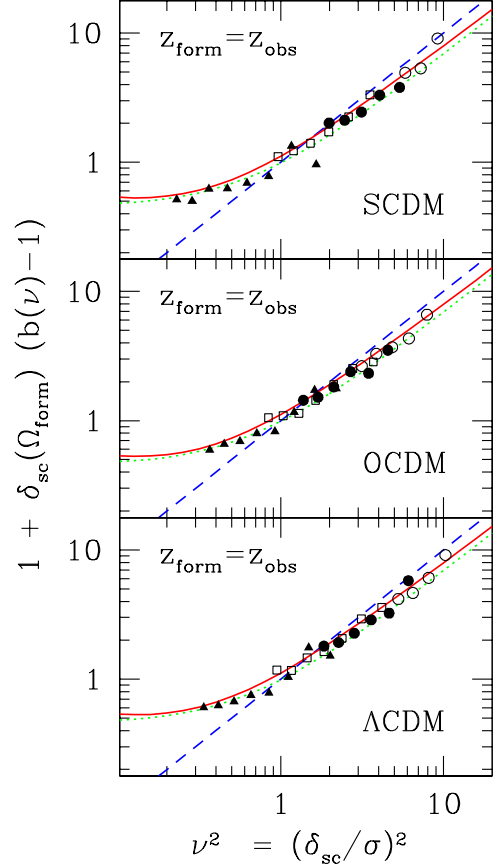


Figure 6. The large scale bias factor $b(m)$ as a function of halo mass in the GIF simulations. Dashed curves show the spherical collapse prediction of Mo & White (1996), dotted curves show the peak background split formula of Sheth & Tormen (1999), and solid curves show the ellipsoidal collapse prediction of this paper.

in the scale free simulations. Since this difference is small, we have not pursued this further.)

We end this section with a brief comparison of the ellipsoidal collapse bias relation with that in simulations which started from realistic initial power spectra. Sheth & Tormen (1999) showed that in the GIF simulations of SCDM, Λ CDM and OCDM models, the bias relation for haloes which are defined at z_{form} and are observed at $z_{\text{obs}} = z_{\text{form}}$ could be rescaled to produce a plot that was independent of z_{form} (see their Fig. 4). The symbols in Fig. 6 show this rescaled bias relation for $z_{\text{form}} = 0, 1, 2$, and 4 (filled triangles, open squares, filled circles, and open circles, respectively). The dashed curves show the standard spherical collapse prediction, the dotted curves show the bias relation associated with the peak background split, and the solid curves show the ellipsoidal collapse prediction. These GIF simulations span a smaller range in $\delta_{\text{sc}}/\sigma$ than Jing’s $n = -0.5$ scale free runs. Over this smaller range, the peak background split formula and the moving barrier prediction are both in good agreement with the simulations.

5 DISCUSSION

The mass function measured in simulations (equation 6) is different from that (equation 2) predicted by Press & Schechter (1974) and by the excursion set approach of Bond et al. (1991) and Lacey & Cole (1993). If a model does not predict the mass function accurately, then the other model predictions, such as the large scale halo-to-mass bias relation, will also be inaccurate (e.g. Sheth & Lemson 1999a; Sheth & Tormen 1999). It is important that a model describe both these statistical quantities accurately if the mass dependence of the abundance and spatial correlations of objects are to provide useful constraints on cosmological parameters (e.g. Mo, Mao & White 1999; Arnouts et al. 1999; Moscardini et al. 1999). Since the excursion set approach allows one to make many analytic estimates about the evolution of hierarchical clustering relatively easily, it is worth modifying the original model so that it reproduces the simulation mass function. The hope is that, if it predicts this accurately, the other predicted quantities will also be accurate.

All predictions of the excursion set approach are based on solving problems associated with the time which passes before a particle undergoing Brownian motion is first absorbed onto a barrier. The predicted mass function depends on the height of the absorbing barrier as a function of random walk time. Therefore, it is crucial to model this height accurately. Bond et al. (1991) argued that a barrier of constant height is associated with the dynamics of spherical collapse. Section 2.2 of the present paper showed that combining the ellipsoidal collapse model for the dynamics with the assumption that the initial fluctuation field was Gaussian produces a barrier shape that is not constant (equation 4). Rather, it has a shape that is very similar to that which is necessary to produce a mass function like the one in numerical simulations (equation 7): it increases with decreasing mass.

Our discussion of the excursion set approach in Section 3 allowed us to demonstrate that the inclusion of ellipsoidal dynamics (i.e., requiring that less massive objects be more overdense to collapse by a given time) reduces dramatically the scatter between the halo mass predicted by the theory and that which a halo actually has in simulations (Figs. 2–4). That is, we showed explicitly that the ellipsoidal collapse, moving barrier, excursion set predictions work well on an object-by-object basis. We then used the barrier crossing statistics of independent unconstrained random walks to provide an estimate of the halo mass function. Providing a more exact relation between the first crossing distribution of such walks and the mass function is the subject of ongoing work. Even in this simple approximation, however, we argued that the approach also works well in a statistical sense. It predicts a mass function that has the same shape as the one in the simulations. In addition, in contrast to the constant, spherical collapse barrier, our moving ellipsoidal collapse barrier predicts a large scale halo-to-mass bias relation (equation 8) that is similar to the one measured in simulations, even at the low mass end (Figs. 5 and 6).

We are not the first to consider the effects of non-spherical dynamics on the shape of the mass function of bound objects. Whereas Monaco (1995; 1997a,b), Audit, Teyssier & Alimi (1997) and Lee & Shandarin (1998) have

studied models in which the initial deformation tensor is used to compute approximations to the collapse time, Bond & Myers (1996) combined the information contained in the deformation tensor with the ellipsoidal collapse model to estimate the epoch of collapse. With the exception of Monaco, who assumed that virialization is associated with collapse of a single axis, all the other authors agree that it is the collapse of all three axes that is more relevant. We agree. As a result of his definition, Monaco found that the ‘moving’ barrier should decrease, rather than increase, with decreasing mass. One consequence of this is that if the barrier has the shape required by Monaco, then the inclusion of ellipsoidal dynamics would increase rather than decrease the scatter in our Fig. 3, relative to that associated with the ‘standard’ spherical collapse model.

We feel that our analysis incorporates some but not all of the various useful results derived by the authors cited above. For example, we could have computed the mass function following the ‘fuzzy’ threshold approach of Audit, Teyssier & Alimi (1997) and Lee & Shandarin (1998). In this approach, the ‘standard’ spherical model corresponds to one in which all regions denser than a certain value δ_{sc} collapse: $p(\text{collapse}|\delta)$ is a step function. Audit, Teyssier & Alimi and Lee & Shandarin provide various different definitions of this collapse probability, which are all motivated by combining approximations to non-spherical dynamics with the statistics of the initial shear field. Figs. 2 and 3 of those papers show that, in such models, the probability of collapse is not a sharp step function. For our definition of collapse,

$$p(\text{collapse}|\delta) = \int_0^\infty de \int_{-e}^e dp g(e, p|\delta) \Theta(\delta - \delta_{ec}(e, p))$$

is not a step function either. It is fairly straightforward to compute this probability using the results given in Section 2.2. However, we feel that the excursion set approach allows one to estimate many more useful quantities than this fuzzy threshold approach. This is why we have chosen to use our formula for $\delta_{ec}(e, p)$ to compute a moving barrier shape, rather than to pursue the fuzzy threshold approach further.

Another place where we could have done a more detailed calculation but did not is in relating mass and ellipticity. We used equation (A4) to provide a deterministic relation between $\sigma(m)$ and e , whereas there is considerable scatter around this relation. The authors cited above describe various methods for incorporating the effects of this scatter. In principle, we could apply any of their methods to our definition of collapse, and so include the effects of the scatter around the relation we use for translating $\delta_{ec}(e, p, z)$ of Fig. 1 to the moving barrier shape $B(\sigma, z)$ of equation (4). [For example, equations (24) and (28) of Audit, Teyssier & Alimi (1997) provide what is essentially their formula for what we call $B(\sigma, z)$, and their equation (29) is an estimate for the scatter.] Whereas this might allow one to include the effects of the stochasticity resulting from a Gaussian fluctuation field more accurately (and so might allow one to reduce the scatter in Fig. 3), this increase in rigour is at the cost of making the other predictions associated with the excursion set model more difficult to compute. This is why we have not pursued this further.

In this respect, our approach is more practical than rigorous. Because we are less careful than others about the exact stochasticity and dynamics, our approach (to provide

an accurate fitting function to the barrier shape) is, perhaps, easier to implement. Indeed, we think it important to stress that, while it is reassuring that the barrier shape associated with the GIF mass function can be understood within the context of a slightly more sophisticated treatment (than the spherical model) of the dynamics of collapse, the various other predictions of the excursion set model (the conditional mass function, the forest of merger history trees, and the nonlinearity and stochasticity of the halo-to-mass bias relation) are sufficiently useful, and sufficiently easy to make once the barrier shape is known, that they are worth making, using the fitting function of equation (7), whether or not a more careful analysis of the dynamics of collapse and the stochasticity of the initial fluctuation field yields exactly the same barrier shape. The results presented in Section 4 provide sufficient justification for using the barrier shape in this way. Making more such predictions is the subject of work in progress.

Before concluding, we should mention that our moving barrier approach suggests that less massive objects at a given time must form from regions which are initially more overdense than the regions from which the more massive objects formed. This is in the same qualitative sense as the relation between mass and central-concentration that is measured for evolved halo density profiles (Navarro, Frenk & White 1997). These authors argue that less massive haloes are more centrally concentrated because, on average, the mass of less massive haloes was assembled earlier, at a time when the universal background density was higher. Our results suggest that at least some of this relation is built in.

ACKNOWLEDGMENTS

Thanks to Tom Theuns for discussing how our formulae for ellipticity and prolateness are related to the Bardeen et al. formulae for peaks.

REFERENCES

- Arnouts S., Cristiani S., Moscardini L., Matarrese S., Lucchin F., Fontana A., Giallongo E., 1999, MNRAS, submitted, astro-ph/9902290
- Audit E., Teyssier R., Alimi J.-M., 1997, A&A, 325, 439
- Bardeen J.M., Bond J.R., Kaiser N., Szalay A., 1986, ApJ, 304, 15
- Bernardeau F., 1994, ApJ, 427, 51
- Bond J. R., Cole S., Efstathiou G., Kaiser N., 1991, ApJ, 379, 440
- Bond J. R., Myers S., 1996, ApJS, 103, 1
- Catelan P., Lucchin F., Matarrese S., Porciani C., 1998, MNRAS, 297, 692
- Doroshkevich A. G., 1970, Astrofizika, 3, 175
- Hoffman Y., Shaham J., 1985, ApJ, 297, 16
- Icke V., 1973, A&A, 27, 1
- Jing Y., 1998, ApJL, 503, L9
- Jing Y., 1999, ApJL, 515, L45
- Kauffmann G., Colberg J.M., Diaferio A., White S.D.M., 1999, MNRAS, 303, 188
- Lacey C., Cole S., 1993, MNRAS, 262, 627
- Lacey C., Cole S., 1994, MNRAS, 271, 676
- Lee J., Shandarin S., 1998, ApJ, 500, 14
- Lemson G., 1993, MNRAS, 263, 913
- Lemson G., 1995, PhD. thesis, Univ. of Groningen
- Mo H. J., White S. D. M., 1996, MNRAS, 282, 347
- Mo H. J., Jing Y., White S. D. M., 1996, MNRAS, 282, 1096
- Mo H. J., Jing Y., White S. D. M., 1997, MNRAS, 284, 189
- Mo H. J., Mao S., White S. D. M., 1999, MNRAS, 304, 175
- Monaco P., 1995, ApJ, 447, 23
- Monaco P., 1997a, MNRAS, 287, 753
- Monaco P., 1997b, MNRAS, 290, 439
- Monaco P., 1999, in Observational Cosmology: The Development of Galaxy Systems, ed. Giuricin et al., ASP Conf. Ser
- Moscardini L., Matarrese S., De Grandi S., Lucchin F., 1999, MNRAS, submitted, astro-ph/9904282
- Navarro J. F., Frenk C. S., White S. D. M., 1997, ApJ, 490, 493
- Porciani C., Catelan P., Lacey C., 1999, ApJ, 513, L99
- Press W., Schechter P., 1974, ApJ, 187, 425
- Sheth R. K., 1996, MNRAS, 281, 1277
- Sheth R. K., 1998, MNRAS, 300, 1057
- Sheth R. K., Lemson G., 1999a, MNRAS, 304, 767
- Sheth R. K., Lemson G., 1999b, MNRAS, 305, 946
- Sheth R. K. & Tormen G., 1999, MNRAS, in press, astro-ph/9901122
- White S. D. M., Frenk C., 1991, ApJ, 379, 52
- White S. D. M., Rees M., 1978, MNRAS, 183, 341
- White S. D. M., Silk J., 1979, ApJ, 231, 1
- White S. D. M., 1996, in Schaeffer R. et al., eds, Cosmology & Large-scale Structure, Proc. 60th Les Houches School, Elsevier, p.349

APPENDIX A: GAUSSIAN RANDOM FIELDS

Consider a Gaussian random field smoothed on scale R_f . Let $\sigma(R_f)$ denote the rms fluctuation of the smoothed field. Any position in this field has an associated perturbation potential, the second derivatives of which define what, in the Zeldovich approximation, is called the deformation tensor. Let $\lambda_1 \geq \lambda_2 \geq \lambda_3$ denote the eigenvalues of this tensor. Different positions in the smoothed field will have different λ_i s. The probability $p(\lambda_1, \lambda_2, \lambda_3)$ that the eigenvalues are $\lambda_1 \geq \lambda_2 \geq \lambda_3$, in that order, is

$$p(\lambda_1, \lambda_2, \lambda_3) = \frac{15^3}{8\pi\sqrt{5}\sigma^6} \exp\left(-\frac{3I_1^2}{\sigma^2} + \frac{15I_2}{2\sigma^2}\right) \times (\lambda_1 - \lambda_2)(\lambda_2 - \lambda_3)(\lambda_1 - \lambda_3), \quad (\text{A1})$$

where $\sigma \equiv \sigma(R_f)$, $I_1 \equiv \lambda_1 + \lambda_2 + \lambda_3$, and $I_2 \equiv \lambda_1\lambda_2 + \lambda_2\lambda_3 + \lambda_1\lambda_3$ (Doroshkevich 1970). In the linear regime, the initial density fluctuation is δ , and because it is related to the potential by Poisson's equation, $\delta \equiv I_1$. By integrating $p(\lambda_1, \lambda_2, \delta - \lambda_1 - \lambda_2)$ over $(\delta - \lambda_1)/2 \leq \lambda_2 \leq \lambda_1$, and then over $\delta/3 \leq \lambda_1 \leq \infty$, where the limits of integration follow from the fact that the eigenvalues are ordered, it is straightforward to verify that the distribution of δ is Gaussian, with variance σ^2 . Also, since $\sigma^2 \ll 1$ in linear theory, $|\delta| \ll 1$ almost surely, so the smoothing scale R_f has an associated mass $M \propto R_f^3$.

It is usual to characterize the shape of a region by its ellipticity, e , and prolateness, p , where

$$e = \frac{\lambda_1 - \lambda_3}{2\delta}, \quad \text{and} \quad p = \frac{\lambda_1 + \lambda_3 - 2\lambda_2}{2\delta} \quad (\text{A2})$$

(e.g., Bardeen et al. 1986). If we use the λ s from the formulae above, then the e and p values we obtain are those associated with the potential, rather than the density field. (So our e and p are what Bond & Myers 1996 denoted e_v and p_v , and

they are not the same as what Bardeen et al. 1986 call e and p .) The ordering of the eigenvalues means that $e \geq 0$ if $\delta > 0$, and $-e \leq p \leq e$. A spherical region has $e = 0$ and $p = 0$. Using equation (A2) in Doroshkevich's formula allows one to write down the distribution of e and p given δ . Let $g(e, p|\delta) de dp$ denote this distribution. Then

$$g(e, p|\delta) = \frac{1125}{\sqrt{10\pi}} e (e^2 - p^2) \left(\frac{\delta}{\sigma}\right)^5 e^{-\frac{5}{2} \frac{\delta^2}{\sigma^2} (3e^2 + p^2)}, \quad (\text{A3})$$

where we have used the fact that converting from $d\lambda_1 d\lambda_2 d\lambda_3$ to $d\delta de dp$ introduces a factor of $2/3$ (Bardeen et al. 1986). It is easy to verify that integrating this over $-e \leq p \leq e$, and then over $0 \leq e \leq \infty$ gives unity, provided $\delta > 0$. For all e , this distribution peaks at $p = 0$. When $p = 0$, the maximum occurs at

$$e_{\text{mp}}(p = 0|\delta) = (\sigma/\delta)/\sqrt{5}. \quad (\text{A4})$$

This provides a monotonic relation between e_{mp} and δ/σ . Also, $e_{\text{mp}} \rightarrow 0$ as $\delta/\sigma \rightarrow \infty$: for a given R_f denser regions are more likely to be spherical than less dense regions, whereas, at fixed δ , larger regions are more likely to be spherical than smaller ones. In general, the most probable shape of a randomly chosen region in a Gaussian random field is triaxial, with $p \approx 0$. Therefore, since we are interested in objects that form from Gaussian fluctuations, we must study the collapse of ellipsoids with $e \geq 0$. Requiring that the initial regions of interest be peaks does not change these qualitative conclusions, though there are quantitative differences. Equations (7.6) and (7.7) of Bardeen et al. (1986) give the expressions corresponding to g and e_{mp} for peaks (but note that their expressions are for the density, rather than the potential field).